Engineering of a Blocking Layer Structure for Low-Lag Operation of the a-PbO-Based X-Ray Detector

Oleksandr Grynko, *Graduate Student Member, IEEE*, Tristen Thibault, Emma Pineau, and Alla Reznik

***Abstract*— Direct conversion flat panel detectors are of great significance to the field of medical X-ray imaging since they offer imaging performance and diagnostic capabilities not achievable with other methods. Currently, mammographic direct conversion detectors employ a layer of amorphous selenium (a-Se) photoconductor. Although its properties ideally fit the requirements of mammography, where "soft" X-rays are used, a-Se cannot be used in high-energy X-ray procedures. To extend the diagnostic capabilities of the direct conversion detectors, amorphous lead oxide (a-PbO) is proposed as an alternative photoconductor. It is a high effective atomic number material and thus has a higher X-ray stopping power over the wide X-ray energy range. a-PbO is, therefore, a suitable candidate for applications in radiography, fluoroscopy, and digital tomosynthesis. Here, we report on the development of a blocking structure with a polyimide (PI) layer needed to maintain low dark current at high electric fields. We demonstrate that a 1-μm-thick PI blocking layer allows the operation of the detector at strong electric fields ($\geq$10 V/μm) while suppressing the dark current to an innocuous level (<1 pA/mm^2). It also improves temporal performance by reducing signal lag. No ghosting effect was observed at exposure rates up to 1 R/s; however, at high radiation levels, the detector's sensitivity degraded. This degradation is not permanent as the detector restores its original sensitivity after several hours of rest in the dark without bias applied.**

***Index Terms*— Blocking layer, direct conversion, lead oxide, polyimide, X-ray detectors.**

I. Introduction

THE most common and important application of fluoroscopic X-ray imaging today is in image-guided diagnostic and therapeutic procedures where real-time (30 frames/s) image sequences are used to guide the interventional radiologist's mind and hands. The current state-of-the-art X-ray imaging technology for diagnostic X-ray energies is based on an indirect conversion method where a scintillator (e.g., CsI or Gd_2O_2S) first converts X-ray quanta into optical photons, which in turn diffuse through a phosphor and then are converted to electrons by an array of photodiodes [1]. This two-step conversion process reduces the X-ray-to-charge conversion gain, and as a result, these detectors are quantum limited, so the signal-to-noise ratio (SNR) for a given pixel is proportional to the square root of the number of detected X-rays. Subsequently, at the lowest exposure levels common in fluoroscopy (0.1–1 μR/frame), the electronic noise dominates the quantum noise and, therefore, visibility of low-contrast objects is compromised. Additionally, the omnidirectional propagation of optical photons in the scintillator reduces the spatial resolution of the indirect conversion detectors [2], [3].

These issues can be overcome by the use of the direct conversion approach. "Direct conversion" means that X-rays are absorbed in a photoconductor that directly creates electron–hole pairs that are subsequently separated by an applied electric field to generate a recordable signal [4], [5]. The charges are moved by a field making it possible to create an image with a thick detector layer without significant loss of resolution. Commercial direct conversion flat panel X-ray imagers (FPXIs) are used in breast imaging, i.e., in the mammography energy range, where they demonstrate superior image quality in comparison with the indirect conversion scheme [5], [6].

Two major components of FPXIs are a large-area thin-film transistor (TFT) or complementary metal–oxide–semiconductor (CMOS) active matrix array [7] (as used in flat panel displays, for example) and a photoconductive layer which is deposited directly onto the imaging array and acts as an X-ray-to-charge transducer. Currently, commercial FPXIs employ a layer of stabilized amorphous selenium (a-Se) photoconductor. Due to the low atomic number ($Z = 34$) of selenium, a-Se-based detectors are efficient only for low-energy X-rays used in mammography. To extend the diagnostic capabilities of the direct conversion detectors over radiographic, fluoroscopic, and digital breast tomosynthesis (DBT) energy range, a-Se has to be replaced with high-Z, wide bandgap X-ray photoconductive material. In addition, for real-time applications, an X-ray photoconductor has to demonstrate an adequate temporal performance in terms of signal lag

Manuscript received January 18, 2021; revised February 26, 2021; accepted March 17, 2021. Date of publication March 29, 2021; date of current version April 22, 2021. This work was supported in part by Teledyne DALSA, the Natural Sciences and Engineering Research Council of Canada (NSERC) and Mitacs. *(Corresponding author: Oleksandr Grynko.)*

Oleksandr Grynko is with the Chemistry and Materials Science Program, Lakehead University, Thunder Bay, ON P7B 5E1, Canada (e-mail: ogrynko@lakeheadu.ca).

Tristen Thibault and Emma Pineau are with the Physics Department, Lakehead University, Thunder Bay, ON P7B 5E1, Canada (e-mail: ttthibau@lakeheadu.ca; enpineau@lakeheadu.ca).

Alla Reznik is with the Physics Department, Lakehead University, Thunder Bay, ON P7B 5E1, Canada, and also with the Thunder Bay Regional Health Research Institute, Thunder Bay, ON P7B 6V4, Canada (e-mail: areznik@lakeheadu.ca).

Color versions of one or more figures in this article are available at https://doi.org/10.1109/TED.2021.3067616.

Digital Object Identifier 10.1109/TED.2021.3067616

(i.e., a postsignal after X-ray irradiation): the lag should not exceed that of the scintillators. This is a strict requirement, since in the state-of-the-art indirect conversion detectors lag is imperceptible. Indeed, the CsI-based detector with an a-Si TFT imager designed for cardiac imaging demonstrated the first frame lag of 2% (30 frames/s readout) [8]. An indirect detector with a Gd_2O_2S scintillator and a-Si:H TFT array showed a 2% lag after the lowest frame time of 0.2 s [9]. A more prominent example of the indirect conversion detector utilizes an advanced imaging array based on the CMOS technology and demonstrates the first frame lag below 0.1% at 30 frames/s [10].

Several photoconductors have been intensively investigated for this role over the last two decades, but a large signal lag deemed them unapplicable for further consideration as X-ray-to-charge transducers in dynamic X-ray imaging: poly-PbI_2 (first frame lag ~30%–50% [11], [12]), poly-HgI_2 (first frame lag ~10%–20% [11]–[13]), poly-CdTe (lag at the first frame ~6%–20% [14], [15] and ~30% after 0.5 s for the detector with CMOS imager [16]), poly-CdZnTe (first frame lag ~6%–70% [17], [18]), and poly-PbO (1.5%–7% lag after 1 s [19], [20]). Another candidate for the X-ray-to-charge transducer in direct conversion detectors is the perovskites, a new family of emerging materials. Although promising, at least at the very early stage of their development, perovskites also demonstrate large signal lag [21]. If this problem is not solved, all the efforts in the development of perovskite technology will come to naught.

So far, the only direct conversion detectors that can be considered for dynamic imaging are based on the a-Se photoconductor. Indeed, although the main application of a-Se-based detectors was in static mammographic imaging, its performance was also evaluated for real-time applications in dynamic imaging, such as fluoroscopy and digital subtraction angiography (DSA). It typically exhibited a first frame lag at 30 frames/s of 2%–6% [14], [22], [23], but a faster response (lag $< 1\%$) was also reported [24]–[26].

One of the possible alternatives to a-Se with nearly lag-free operation is amorphous lead oxide (a-PbO) [27], [28]. It is a photoconductive material with a fast response, a potentially higher charge yield, higher effective atomic number ($Z_{\text{eff}} \approx 79$), and higher X-ray stopping power over a wide energy range [27], [28]. Indeed, for energies relevant to medical X-ray imaging, the attenuation coefficient for a-PbO ranges from 704 cm^{-1} at 20 keV to 20 cm^{-1} at 140 keV, in comparison to 210 and 1.3 cm^{-1} for a-Se for the same energies, respectively [29]. Since a-PbO is proposed as a substitute for a-Se in X-ray digital detectors with a high dynamic range, an urgent problem arises to minimize the dark current and to develop an a-PbO blocking layer structure, similar to how it was achieved in a-Se.

The need for blocking structures arises from the strong electric field applied to the X-ray-to-charge transducer during detector operation. Typically, a field of 10 V/μm or higher must be applied to a photoconductor to achieve an acceptable charge collection efficiency. If preventive measures are not taken, the application of such a high electric field might lead to the excessive injection of the charge carriers from the contacts into the photoconductor, causing a high dark current, subsequent deterioration of the SNR, and degradation of the visibility of low-contrast objects at low exposures. In addition, the dark carriers may be trapped in the bulk of the photoconductor, thus modifying the internal electric field and affecting the photogeneration efficiency across the layer. An acceptable dark current density for X-ray detectors should preferably not exceed 1–10 pA/mm^2, depending on the clinical application [5].

Since the thermal generation of carriers in wide bandgap photoconductors used in imaging detectors is typically very small, the main source of dark current is attributed to an injection of carriers from the electrodes [30]. A practical approach to minimize the injection and to reduce the dark current to an acceptable level is to introduce thin blocking layers between the photoconductor and the electrodes [31], [32].

In a-Se-based detectors, these blocking layers (with thicknesses much smaller than the photoconductor thickness) are made from specially alloyed and doped a-Se. The doping is designed to not only cause deep trapping of carriers injected from the adjacent electrodes but also to allow the opposite sign carrier to be transported at the same time. By analogy with semiconductors, hole and electron blocking layers are called n-like and p-like layers, respectively. The dark current in such multilayer a-Se photoconductors is about 3 orders of magnitude smaller than that in a single a-Se layer with the same thickness and applied field [32].

An alternative approach to prevent injection is to use blocking layers made of a semi-insulating polymer, like cellulose acetate (CA) [33] or polyimide (PI) [24]. It was previously shown that both CA and PI polymers are compatible with a-Se technology and can serve as blocking layers in a-Se avalanche structures: the CA layer improves stability against dielectric breakdown, while the carrier mobilities are not compromised. As for PI, it bonds well to a-Se, it is compatible with a-Se deposition technology, and it enables stable operation at low dark currents without sudden breakdown and associated structural transformations. In addition, PI acts as a soft buffer layer reducing shear strain at the photoconductor–substrate interface and improves adhesion [34]. Similar to n-like and p-like layers in the a-Se blocking structure, these polymers would need to prevent the injection of one type of carriers from the electrode while allowing the collection of photogenerated carriers of the opposite sign. If the last condition is not met, the carriers will be trapped at the interface causing screening of the electric field and reduction of the detector's charge collection efficiency. Additionally, it can result in the degradation of temporal performance through increased lag and ghosting effects (i.e., change in X-ray sensitivity due to previous irradiation).

Here, we report on our approach to a-PbO blocking structures with a thin layer of PI. This polymer layer can be easily and cost-efficiently applied even to large-area substrates using a standard spin-coating technique. Its charge blocking properties can be tuned by varying the thickness of the layer.

Although the use of a PI blocking layer in a-Se avalanche detectors is very encouraging for an application of PI in conjunction with the a-PbO photoconductor, concerns remain

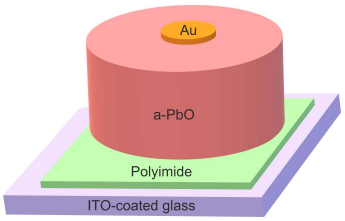

Fig. 1. Schematic of the PI/a-PbO blocking structure.

TABLE I
PI LAYER COATING AND CURING PARAMETERS

Spin-coating			
	Step 1	Step 2	Step 3
Duration, s	5	30	7
Speed, rpm	500	6000	0
Acceleration, rpm per s	550	990	-1100

Curing	
Curing temperature, °C	350
Curing duration, min	30
Heating-cooling rate, °C/min	4
Nitrogen flow, sL/min	2

regarding the possible degradation of temporal performance of a PI/a-PbO detector as often happens if a "foreign" layer is introduced into the structure. However, by investigating the kinetics of the dark current, signal lag, and ghosting, we demonstrate that no deterioration of temporal performance is observed, while the dark current is reduced to an innocuous level. The above-mentioned features make PI a practical approach for the development of a-PbO-based X-ray digital detectors with a low dark current for a variety of applications.

II. METHODS

A. Sample Preparation

The PI/a-PbO blocking layer structure is schematically shown in Fig. 1. In this configuration, a thin layer of PI was applied (under controlled parameters like spin speed and duration, curing temperature and time) to the ITO-coated glass prior to the deposition of the a-PbO layer.

The sample was prepared in a cleanroom environment as follows. Commercially supplied ITO-coated glass was sequentially cleaned with acetone, methanol, isopropanol, and dry nitrogen, and then placed for 10 min on the hot plate heated to 90 °C to remove any remaining solvents. A polyamic acid precursor dissolved in an n-methyl-2-pyrrolidone (NMP)-based solvent was dispensed in the center of the stationary substrate. To obtain a 1-μm-thick layer of PI, a spin coating was carried out in three steps with parameters shown in Table I. In the first step, the substrate is spun at a low speed to allow the precursor to spread across the entire surface of the substrate. After that, the substrate is accelerated to a final speed, which is the main factor in the determination of the resulting PI layer thickness. After spinning, it is decelerated to a static state. The spin duration in the first step and the acceleration in the second step were adjusted to obtain a uniform thickness across the surface. After spin coating, the substrate was placed on a hot plate, ramped to a high temperature (sufficient for complete dissociation of the NMP solvent carrier and full imidization of the PI film) and cured under constant dry nitrogen flow with parameters shown in Table I.

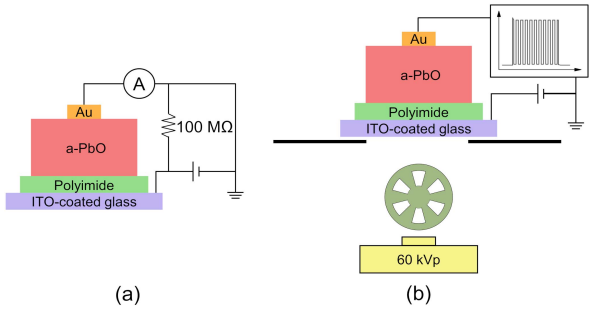

Fig. 2. Schematic experimental setup for (a) dark current kinetics measurement and (b) temporal performance characterization.

In order to be able to make an electrical connection to the ITO side of the substrate, which is essential for electrical and X-ray characterization of the detector described further in the text, the edges of the substrate were masked with a Kapton PI tape prior to the spin coating. The tape was peeled off after the coating.

A 19-μm-thick layer of a-PbO was deposited afterward by the ion-assisted thermal evaporation technique with the following parameters: base pressure $\sim 5 \times 10^{-5}$ Pa, process pressure $\sim 6 \times 10^{-2}$ Pa, furnace temperature $\sim$1000 °C, substrate temperature $\sim$100 °C, deposition rate $\sim$0.2 μm/min, ion energy $\sim$50 eV, and ion flux $\sim$0.2 mA/cm^2. A detailed description of the deposition process can be found in [35]. Finally, a gold contact, 20 nm in thickness and 1 mm in diameter, was sputtered atop of the a-PbO in a dedicated chamber.

B. Dark Current Kinetics Measurement

Dark current was measured as a function of time for different bias voltages relevant to the direct conversion detector operation [Fig. 2(a)]. The sample was placed in a light-tight shielded box to prevent photogeneration. A positive voltage (Stanford Research Systems PS350 power supply) was applied to the ITO electrode, and the dark current was read out from the Au electrode with Keithley 35617EBS electrometer. A power supply and an electrometer were connected through a GPIB interface (Tektronix AD007) to a host computer which provided control and data acquisition. A 100-MΩ resistor was connected in parallel to the sample to allow the recovery current to flow in a circuit in between the measurements.

Prior to measurement, the sample was short-circuited in the dark for at least 10 h to allow complete detrapping of charge carriers. The voltage was ramped at a rate of 5 V/s, and the dark current was read out every second during a 2-h period. After the decay is recorded, the voltage was ramped to 0 V at the same rate and the detector is left unbiased for 10 h.

C. Temporal Performance Characterization

The main goal of this work is to investigate the impact of the PI blocking layer on the temporal performance of a-PbO-based X-ray detector and to evaluate signal lag and ghosting

effects. Signal lag is the residual current after the termination of X-ray irradiation and ghosting is the degradation of the detector's sensitivity as a result of previous irradiation. In order to evaluate the detector's temporal performance in near clinical conditions, it is necessary to irradiate it with a sequence of short X-ray pulses (with a rate up to 30 frames/s) and to measure the current during the irradiation and with X-rays OFF.

The characterization was carried out using the X-ray-induced photocurrent method (XPM) in a pulsed mode, where a rotating chopper was used to modulate an X-ray pulse at a variable frequency. The experimental setup is shown in Fig. 2(b). A sample is placed in the shielded aluminum box. Prior to measurement, the sample was short-circuited in the dark for at least 2 h to allow complete detrapping of charge carriers. A positive dc bias was applied to the ITO from a high-voltage power supply (Stanford Research Systems PS350), and the photocurrent was readout from the Au electrode on an oscilloscope (Tektronix TDS 2024C) with 1-MΩ native input resistance. A bias was applied to the sample for 10 min prior to irradiation to allow the dark current to stabilize and drop to a level below 5 pA/mm^2. The X-ray tube (Dunlee PX1412CS, insert DU-304) with a Tungsten target was used to generate 1-s-long 60-kVp X-ray pulses. At this energy and thickness of the sample, the detector has an absorption efficiency of 25%. A 1.3-mm Al filter was used to attenuate low-energy photons and minimize Compton backscattering noise, and a 2-mm lead collimator was used to prevent stray scattering. The exposure was monitored by the Keithley 96035 ionization chamber; attenuation by a glass substrate and a chopper was considered when calculating the total incident on the detector exposure. A chopper controller (Stanford Research Systems SR540) drives a 2-mm-thick copper chopper with an adjustable frequency and a 50% duty cycle.

D. Lag and Ghosting Measurements

To evaluate lag and ghosting, the sample was irradiated with a train of 1-s-long X-ray pulses modulated at a frequency of 5–30 Hz. 20 pulses were fired with an interval of 60 s (interval time was limited by the risk of overheating the X-ray tube).

A typical response to a continuous and modulated X-ray pulse is shown in Fig. 3. The photocurrents with X-rays ON (PC_{ON}) and OFF (PC_{OFF}) for every frame as well as the dark current prior to irradiation (DC) were recorded for each pulse. The first and the last frames were omitted due to asynchronization of the X-ray pulse and the chopper, and the initial overshoot in the X-ray pulse.

Detector's sensitivity (S) is defined as the amplitude of the photocurrent during the irradiation (PC_{ON}), corrected for the DC. The average values of the photo- and dark currents were used for each pulse. Signal lag (Lag) is quantified as a ratio of the photocurrent after irradiation (when a chopper blade blocks X-rays, PC_{OFF}) to the detector's sensitivity. The ghosting effect can be quantified as a relative sensitivity—a ratio of the sensitivity at a given pulse to the initial sensitivity of a well-rested detector. Sensitivity and lag values were calculated for each pulse n as follows:

$$S_n = \langle \mathrm{PC_{ON}} \rangle_n - \mathrm{DC}_n \tag{1}$$

$$\mathrm{Lag}_n = \frac{\langle \mathrm{PC_{OFF}} \rangle_n - \mathrm{DC}_n}{S_n}. \tag{2}$$

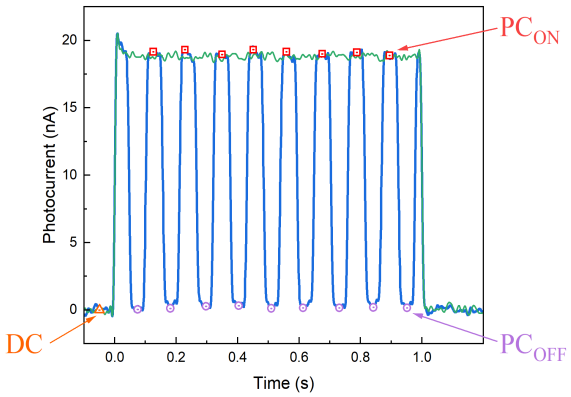

Fig. 3. Typical X-ray response to a continuous and modulated irradiation and measured values within each pulse.

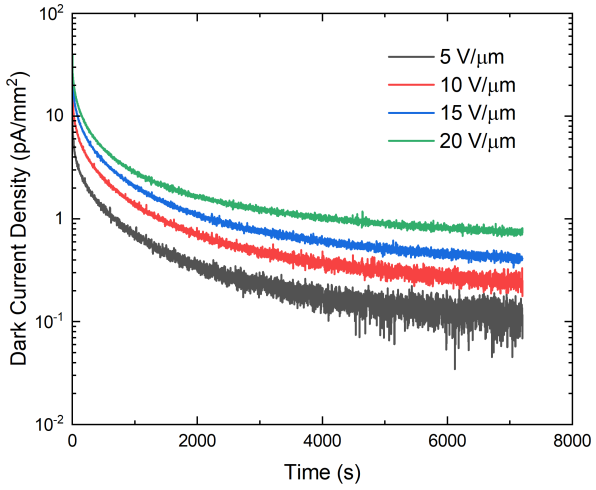

Fig. 4. Kinetics of dark current density at different electric fields.

III. Results and Discussion

A. Dark Current Kinetics Measurement

Fig. 4 shows the decay of the dark current over time at different electric fields (5–20 V/μm). After a bias is applied, the current rapidly decays with time, reducing by nearly 2 orders of magnitude. At 10 V/μm, it drops from 30 to 0.2 pA/mm^2 within 2 hours. However, the dark current increases with the electric field: 0.1 pA/mm^2 at 5 V/μm and 0.7 pA/mm^2 at 20 V/μm after biasing for 2 h.

This behavior is similar to what has been observed in a-Se-based n–i, i–p, and n–i–p blocking structures (where the i-layer is stabilized a-Se), and in PI/a-Se, the dark current rapidly decreases with time by 1–3 orders of magnitude (depending on the layer configuration) over several hours. The lowest attainable steady-state dark current was achieved in n–i–p and PI/a-Se detectors: 0.01–0.05 pA/mm^2 at 10 V/μm [36], [37]. This minimal dark current was attributed

to the bulk thermal generation in the PI/a-Se detector, but in the n–i–p detector, it was assigned to the electron injection [38] or balancing of the carrier trapping and detrapping rates due to Schottky emission over the barrier in the n-layer [39]. Either way, the steady-state dark current in a-Se blocking structures is well below the tolerable level for detector applications of 1 pA/mm^2.

Although further investigation of the dark current kinetics in PI/a-PbO is needed, it can be qualitatively explained in the following model. There are two main sources of the dark current: thermal generation in the bulk of the photoconductor and carrier injection from the electrodes. As PbO has a wide bandgap (~1.9 eV [5]), the bulk thermal generation is relatively small, thus carrier injection is dominant. After the positive bias is applied to the ITO, holes (major carriers in PbO [40]) are injected from the ITO into the PI layer and are accumulated at the ITO/PI interface. This causes screening of the electric field, suppressing further injection, and hence the dark current. After the hole injection is reduced, the electron injection from the negative Au electrode and the thermal generation in the bulk of a-PbO has a dominant effect.

In the PI/a-PbO detector, the dark current did not reached a steady state after 2 hours, meaning that it is not completely suppressed yet. This gives a potential for further dark current reduction. Depending on the mechanism responsible for the final decaying portion of the dark current, it can be achieved by waiting for a longer time (a warm-up period of the detector) or by introducing a second blocking layer into the structure that would prevent the injection of electrons. However, even in the current configuration, an acceptable dark current level of 1 pA/mm^2 can be easily achieved.

B. Temporal Performance

When the detector is exposed to continuous irradiation (Fig. 3), it exhibits a quasi-rectangular response with a constant amplitude and low (<1%) lag. A small overshoot at the beginning of the pulse is a characteristic feature of the X-ray tube, not the detector, since a similar response was observed in the silicon photodiode used to trigger the oscilloscope. A uniform amplitude indicates that the dark current is constant and the photocurrent neither builds-up due to the X-ray triggered injection (as observed, for example, in poly-PbO and early PI/a-Se detectors [20], [24]) nor decreases due to the degradation of the internal electric field caused by the accumulation of X-ray-generated charge at the PI/a-PbO interface. Moreover, when the detector is exposed to modulated irradiation, both the photocurrents during each frame and the amplitude in successive frames remain constant. This indicates the unhindered flow of photogenerated electrons from the photoconductor through the PI layer to the ITO electrode. Indeed, if an accumulation of photogenerated electrons at the interface would occur, a decrease in the photocurrent at the end of each frame would be observed [37]. In [37], a small decrease in the photocurrent during each frame was attributed to a temporary change in the internal electric field, which is restored by hole injection from the anode, keeping the same amplitude of consecutive pulses. Therefore, our analysis of the X-ray response of the PI/a-PbO detector to continuous and modulated irradiation suggests that the presence of the PI layer does not affect charge collection efficiency. This conclusion, together with a suggested mechanism responsible for the dark current kinetics (accumulation of the injected holes from the ITO and screening of the electric field), demonstrates that the PI layer indeed acts as a blocking layer, rather than an insulator.

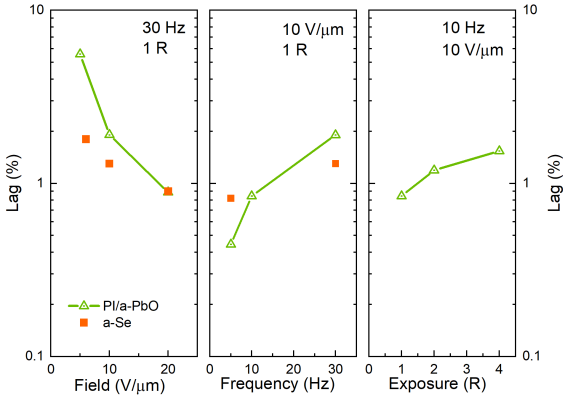

Fig. 5. Signal lag measured as a function of the electric field, modulation frequency and incident exposures in a PI/a-PbO detector. A data set was connected with lines as a guide for the eyes. For the a-Se-based detector, lag values were extracted from the literature.

Fig. 5 shows signal lag values for the PI/a-PbO detector calculated using (2) for various electric fields (5–20 V/μm), modulation frequencies (5–30 Hz), and incident exposures (1–4 R). Signal lag was found to be nearly constant at each pulse (at fixed field, frequency, and exposure); therefore, the values shown have been averaged over 20 pulses.

The application of a stronger electric field improves temporal performance and reduces signal lag. Its value decreases with field: 5.6% at 5 V/μm down to 0.9% at 20 V/μm (with a frequency fixed at 30 Hz). On the contrary, lag increases at higher modulation frequencies and reaches 1.9% at 30 Hz and 10 V/μm. Incident exposure has little effect on the lag in the range investigated, which demonstrates the stability of the X-ray response at different exposure levels. It should be noted that the detector investigated here absorbs only 25% of the incident X-rays under the given beam conditions, thus the absorbed dose by the photoconductor is the only one-quarter of the incident dose.

To compare the temporal performance of a PI/a-PbO detector with an a-Se-based detector, lag values were extracted from [24] and [25] (at the most advantageous bias polarity) and plotted on the same graph. In these works, the lag in a-Se was measured with the same technique and under similar conditions (electric field, modulation frequency, exposure, and interval between pulses); however, the X-ray tube voltage was 28–32 kVp (in contrast to 60 kVp in this work). A blocking layer structure was also used in both a-Se detectors: a PI layer between the photoconductor and the substrate in [24] and two undisclosed blocking layers in [25]. Although the a-Se detector mostly demonstrates a slightly faster response than PI/a-PbO (1.3% and 1.9% lag, respectively, at 10 V/μm, 30 Hz, and 1 R), at the higher field they have a similar performance.

The PI/a-PbO detector exhibits a remarkable improvement of temporal performance over other photoconductors

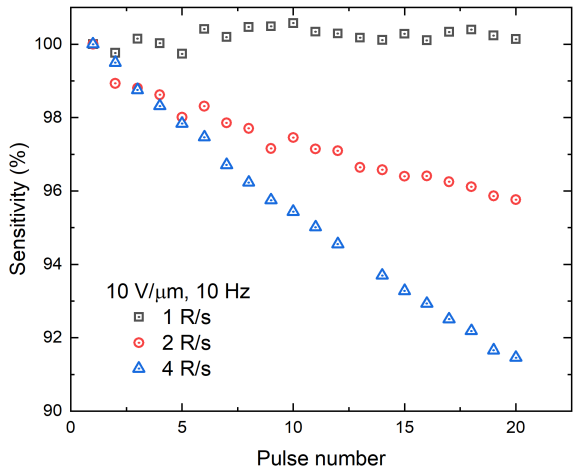

Fig. 6. Degradation of the detector's sensitivity (ghosting) with consecutive pulses at different incident exposure rates.

considered for use in the direct conversion digital detectors (such as polycrystalline layers of PbO, PbI_2, HgI_2, CdTe, CdZeTe, and perovskites) [11]–[21] and marginal signal lag with a-Se [24]–[26], [37] and CsI [8], [10]. So far, a-PbO and a-Se are the only photoconductors where the lag problem was resolved. Combining the high absorption efficiency of PbO in the diagnostic X-ray energy range and the low dark current of the blocking structure, the PI/a-PbO detector has become the most favorable candidate for application in real-time diagnostic imaging.

Degradation of sensitivity for different incident exposure levels is shown in Fig. 6. At the lower exposure rate, sensitivity remains nearly constant showing no ghosting effect. However, at the elevated radiation level, the detector's sensitivity drops with each subsequent pulse. For 4 R/s exposure, the sensitivity decreases by 9% after 20 pulses (an accumulated exposure of 80 R). Note that it is not a permanent degradation of the detector; it restores its initial sensitivity after resting unbiased in the dark for a few hours. Relatively, the a-Se detector had a 10% degradation of sensitivity after 20 R of a cumulative exposure [24] and 15% after 60 R of a cumulative exposure [25].

It should be noted that X-ray doses used here are much larger than those used in the clinical practice [41], [42], and thus represent operation under an extreme load. Indeed, typical exposures to the patient in the dynamic imaging are 0.1–1 R for DBT (accumulated from multiple, usually 9–25, projections over less than 10-s period). For fluoroscopic imaging in surgery, the exposure of some Roentgens can be accumulated over a period of up to few hours. These values of exposure in the patient plane are equivalent to the incident on the detector exposure outside the patient (typically at the periphery of the detector); behind the patient, the exposure would be 10–100 times smaller.

IV. Conclusion

A direct conversion X-ray detector based on the a-PbO photoconductor with a single blocking layer of PI was developed and evaluated. The application process of the PI blocking layer is simple, cost-efficient, and compatible with large-area fabrication. A PI/a-PbO detector satisfies the requirements for low dark current (<1 pA/mm^2) at electric fields as high as 20 V/μm. The detector demonstrates temporal performance suitable for real-time imaging with lag values down to 0.9% at 30 Hz. The detector's response remains constant at a low exposure rate (<1 R/s), but at a high radiation level, the sensitivity degrades. Overall, our approach to use a PI blocking layer in a-PbO-based detector permits the application of a higher electric field for enhanced charge collection and sensitivity, while maintaining suitable temporal and dynamic properties in various clinical and industrial X-ray imaging applications.

Acknowledgment

Financial support from Teledyne DALSA, the Natural Sciences and Engineering Research Council of Canada (NSERC) and Mitacs is gratefully acknowledged.

References

[1] W. Zhao, G. Ristic, and J. A. Rowlands, "X-ray imaging performance of structured cesium iodide scintillators," *Med. Phys.*, vol. 31, no. 9, pp. 2594–2605, Aug. 2004, doi: 10.1118/1.1782676.

[2] M. Simon, K.-J. Engel, B. Menser, X. Badel, and J. Linnros, "Challenges of pixelated scintillators in medical X-ray imaging," *Nucl. Instrum. Methods Phys. Res. A, Accel. Spectrom. Detect. Assoc. Equip.*, vol. 591, no. 1, pp. 291–295, Jun. 2008, doi: 10.1016/j.nima.2008.03.077.

[3] A. Datta, Z. Zhong, and S. Motakef, "A new generation of direct X-ray detectors for medical and synchrotron imaging applications," *Sci. Rep.*, vol. 10, no. 1, p. 20097, Nov. 2020, doi: 10.1038/s41598-020-76647-5.

[4] S. O. Kasap and J. A. Rowlands, "Direct-conversion flat-panel X-ray image sensors for digital radiography," *Proc. IEEE*, vol. 90, no. 4, pp. 591–604, Apr. 2002, doi: 10.1109/JPROC.2002.1002529.

[5] S. Kasap *et al.*, "Amorphous and polycrystalline photoconductors for direct conversion flat panel X-ray image sensors," *Sensors*, vol. 11, no. 5, pp. 5112–5157, May 2011, doi: 10.3390/s110505112.

[6] B. T. Polischuk, S. Savard, V. Loustaneau, M. Hansroul, S. Cadieux, and A. Vaque, "Se-based flat-panel detector for screening mammography," *Proc. SPIE*, vol. 4320, pp. 582–589, Jun. 2001, doi: 10.1117/12.430884.

[7] G. Zentai, "Comparison of CMOS and a-Si flat panel imagers for X-ray imaging," in *Proc. IEEE Int. Conf. Imag. Syst. Techn.*, May 2011, pp. 194–200, doi: 10.1109/IST.2011.5962217.

[8] P. R. Granfors, "Performance characteristics of an amorphous silicon flat-panel X-ray imaging detector," *Proc. SPIE*, vol. 3659, pp. 480–490, May 1999, doi: 10.1117/12.349525.

[9] J. H. Siewerdsen and D. A. Jaffray, "A ghost story: Spatio-temporal response characteristics of an indirect-detection flat-panel imager," *Med. Phys.*, vol. 26, no. 8, pp. 1624–1641, Aug. 1999, doi: 10.1118/1.598657.

[10] L. Korthout *et al.*, "A wafer-scale CMOS APS imager for medical X-ray applications," in *Proc. Int. Image Sensor Workshop Paper*, vol. 70, 2009, pp. 22–28.

[11] R. A. Street *et al.*, "Comparison of PbI_2 and HgI_2 for direct detection active matrix X-ray image sensors," *J. Appl. Phys.*, vol. 91, no. 5, pp. 3345–3355, Mar. 2002, doi: 10.1063/1.1436298.

[12] G. Zentai *et al.*, "Mercuric iodide and lead iodide X-ray detectors for radiographic and fluoroscopic medical imaging," *Proc. SPIE*, vol. 5030, pp. 77–91, Jun. 2003, doi: 10.1117/12.480227.

[13] H. Jiang, Q. Zhao, L. E. Antonuk, Y. El-Mohri, and T. Gupta, "Development of active matrix flat panel imagers incorporating thin layers of polycrystalline HgI_2 for mammographic X-ray imaging," *Phys. Med. Biol.*, vol. 58, no. 3, pp. 703–714, Feb. 2013, doi: 10.1088/0031-9155/58/3/703.

[14] S. Adachi *et al.*, "Experimental evaluation of a-Se and CdTe flat-panel X-ray detectors for digital radiography and fluoroscopy," *Proc. SPIE*, vol. 3977, pp. 38–47, Apr. 2000, doi: 10.1117/12.384511.

[15] K. M. Oh *et al.*, "Improvement of the charge-carrier transport property of polycrystalline CdTe for digital fluoroscopy," *J. Instrum.*, vol. 9, no. 5, May 2014, Art. no. C05033, doi: 10.1088/1748-0221/9/05/C05033.

[16] S. Lee *et al.*, "Direct thermal growth of large scale cl-doped CdTe film for low voltage high resolution X-ray image sensor," *Sci. Rep.*, vol. 8, no. 1, p. 14810, Dec. 2018, doi: 10.1038/s41598-018-33240-1.

[17] S. Tokuda *et al.*, "Experimental evaluation of a novel CdZnTe flat-panel X-ray detector for digital radiography and fluoroscopy," *Proc. SPIE*, vol. 4320, pp. 140–147, Jun. 2001, doi: 10.1117/12.430924.

[18] S. Tokuda, H. Kishihara, S. Adachi, and T. Sato, "Improvement of the temporal response and output uniformity of polycrystalline CdZnTe films for high-sensitivity X-ray imaging," *Proc. SPIE*, vol. 5030, pp. 861–870, Jun. 2003, doi: 10.1117/12.479938.

[19] M. Simon *et al.*, "PbO as direct conversion X-ray detector material," *Proc. SPIE*, vol. 5368, pp. 188–199, May 2004, doi: 10.1117/12.533010.

[20] O. Semeniuk, O. Grynko, G. Decrescenzo, G. Juska, K. Wang, and A. Reznik, "Characterization of polycrystalline lead oxide for application in direct conversion X-ray detectors," *Sci. Rep.*, vol. 7, no. 1, p. 8659, Dec. 2017, doi: 10.1038/s41598-017-09168-3.

[21] G. Kakavelakis, M. Gedda, A. Panagiotopoulos, E. Kymakis, T. D. Anthopoulos, and K. Petridis, "Metal halide perovskites for high-energy radiation detection," *Adv. Sci.*, vol. 7, no. 22, Nov. 2020, Art. no. 2002098, doi: 10.1002/advs.202002098.

[22] W. Zhao, G. DeCrescenzo, S. O. Kasap, and J. A. Rowlands, "Ghosting caused by bulk charge trapping in direct conversion flat-panel detectors using amorphous selenium," *Med. Phys.*, vol. 32, no. 2, pp. 488–500, Jan. 2005, doi: 10.1118/1.1843353.

[23] H. Kawashima, R. Tanaka, K. Ichikawa, K. Matsubara, H. Iida, and S. Sanada, "Investigation of image lag and modulation transfer function in fluoroscopy images obtained with a dynamic flat-panel detector," *Radiol. Phys. Technol.*, vol. 6, no. 2, pp. 367–374, Jul. 2013, doi: 10.1007/s12194-013-0210-9.

[24] S. Abbaszadeh, C. C. Scott, O. Bubon, A. Reznik, and K. S. Karim, "Enhanced detection efficiency of direct conversion X-ray detector using polyimide as hole-blocking layer," *Sci. Rep.*, vol. 3, no. 1, p. 3360, Dec. 2013, doi: 10.1038/srep03360.

[25] B. Zhao and W. Zhao, "Temporal performance of amorphous selenium mammography detectors," *Med. Phys.*, vol. 32, no. 1, pp. 128–136, Dec. 2004, doi: 10.1118/1.1827791.

[26] B. T. Polischuk, Z. Shukri, A. Legros, and H. Rougeot, "Selenium direct-converter structure for static and dynamic X-ray detection in medical imaging applications," *Proc. SPIE*, vol. 3336, pp. 494–504, Jul. 1998, doi: 10.1117/12.317051.

[27] O. Semeniuk, O. Grynko, G. Juska, and A. Reznik, "Amorphous lead oxide (a-PbO): Suppression of signal lag via engineering of the layer structure," *Sci. Rep.*, vol. 7, no. 1, p. 13272, Dec. 2017, doi: 10.1038/s41598-017-13697-2.

[28] O. Grynko, T. Thibault, E. Pineau, G. Juska, and A. Reznik, "Bilayer lead oxide X-ray photoconductor for lag-free operation," *Sci. Rep.*, vol. 10, no. 1, p. 20117, Dec. 2020, doi: 10.1038/s41598-020-77050-w.

[29] J. H. Hubbell and S. M. Seltzer, "Tables of X-ray mass attenuation coefficients and mass energy-absorption coefficients from 1 keV to 20 MeV for elements Z=1 to 92 and 48 additional substances of dosimetric interest (version 1.4)," Nat. Inst. Standards Technol., Gaithersburg, MD, USA, Internal Rep. 5632, Jul. 2004, doi: 10.18434/T4D01F.

[30] M. Z. Kabir *et al.*, "Modeling of dark current and ghosting in multilayer amorphous selenium X-ray detectors," *Proc. SPIE*, vol. 6913, Mar. 2008, Art. no. 69133U, doi: 10.1117/12.770697.

[31] G. Belev and S. O. Kasap, "Reduction of the dark current in stabilized a-Se based X-ray detectors," *J. Non-Crystalline Solids*, vol. 352, nos. 9–20, pp. 1616–1620, Jun. 2006, doi: 10.1016/j.jnoncrysol.2005.11.086.

[32] S. Kasap *et al.*, "Amorphous selenium and its alloys from early xeroradiography to high resolution X-ray image detectors and ultrasensitive imaging tubes," *Phys. Status Solidi (B)*, vol. 246, no. 8, pp. 1794–1805, Aug. 2009, doi: 10.1002/pssb.200982007.

[33] O. Bubon *et al.*, "Electroded avalanche amorphous selenium (a-Se) photosensor," *Current Appl. Phys.*, vol. 12, no. 3, pp. 983–988, May 2012, doi: 10.1016/j.cap.2011.12.023.

[34] S. Abbaszadeh *et al.*, "The effect of the substrate on transient photodarkening in stabilized amorphous selenium," *J. Non-Crystalline Solids*, vol. 358, no. 17, pp. 2389–2392, Sep. 2012, doi: 10.1016/j.jnoncrysol.2011.12.098.

[35] O. Semeniuk, A. Csik, S. Kökényesi, and A. Reznik, "Ion-assisted deposition of amorphous PbO layers," *J. Mater. Sci.*, vol. 52, no. 13, pp. 7937–7946, Jul. 2017, doi: 10.1007/s10853-017-0998-5.

[36] J. B. Frey, K. Sadasivam, G. Belev, H. Mani, L. Laperriere, and S. Kasap, "Dark current–voltage characteristics of vacuum deposited multilayer amorphous selenium-alloy detectors and the effect of X-ray irradiation," *J. Vac. Sci. Technol. A, Vac. Surf. Films*, vol. 37, no. 6, Dec. 2019, Art. no. 061501, doi: 10.1116/1.5121197.

[37] A. Camlica, M. Z. Kabir, J. Liang, P. M. Levine, D. L. Lee, and K. S. Karim, "Use of pulse-height spectroscopy to characterize the hole conduction mechanism of a polyimide blocking layer used in amorphous-selenium radiation detectors," *IEEE Trans. Electron Devices*, vol. 67, no. 2, pp. 633–639, Feb. 2020, doi: 10.1109/TED.2019.2958789.

[38] J. B. Frey, G. Belev, O. Tousignant, H. Mani, L. Laperriere, and S. O. Kasap, "Dark current in multilayer stabilized amorphous selenium based photoconductive X-ray detectors," *J. Appl. Phys.*, vol. 112, no. 1, Jul. 2012, Art. no. 014502, doi: 10.1063/1.4730135.

[39] S. A. Mahmood, M. Z. Kabir, O. Tousignant, H. Mani, J. Greenspan, and P. Botka, "Dark current in multilayer amorphous selenium X-ray imaging detectors," *Appl. Phys. Lett.*, vol. 92, no. 22, Jun. 2008, Art. no. 223506, doi: 10.1063/1.2938888.

[40] O. Semeniuk, G. Juska, J.-O. Oelerich, M. Wiemer, S. D. Baranovskii, and A. Reznik, "Charge transport mechanism in lead oxide revealed by CELIV technique," *Sci. Rep.*, vol. 6, no. 1, p. 33359, Dec. 2016, doi: 10.1038/srep33359.

[41] J. Vilar-Palop, J. Vilar, I. Hernández-Aguado, I. González-Álvarez, and B. Lumbreras, "Updated effective doses in radiology," *J. Radiol. Protection*, vol. 36, no. 4, pp. 975–990, Dec. 2016, doi: 10.1088/0952-4746/36/4/975.

[42] A. M. Asbeutah, A. A. AlMajran, A. Brindhaban, and S. A. Asbeutah, "Comparison of radiation doses between diagnostic full-field digital mammography (FFDM) and digital breast tomosynthesis (DBT): A clinical study," *J. Med. Radiat. Sci.*, vol. 67, no. 3, pp. 185–192, Sep. 2020, doi: 10.1002/jmrs.405.